An Engineered Minidomain Containing an Elastin Turn Exhibits a Reversible Temperature-Induced IgG Binding†

Herald Reiersen and Anthony R. Rees*

Department of Biology and Biochemistry, University of Bath, Claverton Down, Bath BA2 7AY, United Kingdom

Received June 1, 1999; Revised Manuscript Received September 1, 1999

ABSTRACT: A two-helix version of the triple α-helical staphylococcal Protein A, previously shown to retain the Fc binding properties of protein A, has been engineered to contain an elastin sequence, GVPGVG, within the inter-helix turn. The original type I β-turn was replaced with a β-turn from the muscle protein elastin, which has an inverse temperature-induced folding transition. These "elastin mutants" had lost their helical structure, as measured by circular dichroism (CD), and exhibited a lower stability than the wild-type domains (T_m reduced by about 48 °C) in 30% trifluoroethanol. For the wild-type domains, the amount of α-helix and the binding affinity for Fc decreased as the temperature was increased. In contrast, although the starting affinity was lower for the disulfide elastin-turn mutant, it exhibited a 21-fold improvement in affinity over the same temperature range. The melting curve for the elastin-turn minidomain showed cooperative behavior, as measured by the increase in CD-amplitude at 222 nm. The observed CD behavior is consistent with the formation of a type I β-turn, exhibiting similar ΔH and ΔS values to those seen previously for short elastin peptides [Reiersen, H., Clarke, A. R., and Rees, A. R. (1998) *J. Mol. Biol. 283*, 255−264], and accounting for the increase in on-rate. This demonstrates that, when inserted into a stable globular protein, short elastin sequences have the ability to modify local structure and activity, by operating as temperature modulated switches.

One[1] of the applications of protein engineering is the development of novel switch-mechanisms that can regulate and control protein folding and function. There are several naturally occurring mechanisms whereby the activity of a protein can be regulated by conformational change. For example, it may be allosterically modified by binding of a ligand, or as a direct consequence of rearrangements in structure due to covalent modification (e.g., phosphorylation), or as a result of changes in physical or chemical parameters, such as temperature, pH, or degree of hydration (*1*−*3*). The hydration or dehydration of hydrophobic surfaces is a particularly novel mechanism employed to drive conformational changes in elastomeric proteins (*4*−*6*).

In the classical hydrophobic model, water molecules associated with hydrophobic interfaces are structurally ordered and transitions involving hydrophobic hydrated surfaces involve the loss of bound water, or melting of clathrate-like water structures near hydrophobic groups. During protein folding, the loss of water results in an increase in entropy of bulk water accompanied by an increase in protein hydrophobic interactions, providing the driving force for protein function, assembly, stability, and folding (*6*−*10*). Contrary to the behavior of many globular proteins, the elastic muscle protein, elastin, undergoes an inverse temperature transition during hydrophobic dehydration. Polymers derived from elastin and containing repeating $(VPGVG)_n$ sequences ($n \geq 150$) are completely soluble in water below their transition temperatures (∼25 °C) but contract in length by more than 50% with increasing temperature. The free energy released during this transition is sufficient for an elastin fiber to lift more than 1000 times its own mass. The transition involves loss of hydrated water from exposed valine side chains at the higher temperatures, inducing val−val interactions that energize the formation of an ordered β-spiral with three VPGVG units per turn of the spiral, each VPGVG forming a type II β-turn (*4*−*6, 11*).

Formation of the type II β-turn has been verified by different physical and spectroscopic studies, although the presence of other types of β-turns has also been reported (*4*−*6, 12*−*13*). The behavior of the elastin polymers can be regulated by covalent modification, such as phosphorylation, electrochemical reduction of prosthetic groups attached to the polymer, or by the replacement of residues in the sequence by residue types sensitive to pressure, temperature, or pH. Recently, we showed that the behavior of the polymeric elastin can be mimicked by small peptides of 8−28 residues containing the VPGVG sequence in single or multiple copies. This has opened up the possibility of using such sequences in a protein engineering context as molecular "switches" (*11*).

We describe in this paper the first attempt to introduce a temperature switch into a globular protein using the elastin

* Corresponding author. Telephone: +33 466 048666. Fax: +33 466 048667. E-mail:arrees@compuserve.com.

† This work was supported by grants from The Research Council of Norway (No. 110859/410) and DYNAL A/S, Oslo, Norway.

[1] Abbreviations: CD, circular dichroism; DMF (*N*,*N*-dimethylformamide); EDC, *N*-ethyl-*N*′-[(dimethylamino)propyl]carbodiimide; HBS, Hepes buffered saline; HSA, human serum albumin; MRE, $[\theta]_M$, mean residual ellipticity; NHS, *N*-Hydroxysuccinimide; P20, Polysorbate 20; RU, resonance units; SDS, sodium dodecyl sulfate; T_M, transition temperature midpoint; TFA, trifluoroacetic acid; TFE, trifluoroethanol.

10.1021/bi991243a CCC: $18.00
Published on Web 10/21/1999

fragment approach. The target protein was a biologically active fragment of protein A, a multidomain protein from *Staphylococcus aureus* that binds to the Fc region of IgG. Protein A is found on the cell surface of the bacteria and contains a tandem repeat of five different but homologous binding domains, each of approximately 60 residues in a three-helix bundle and designated E, D, A, B, and C (*14*). A synthetic version of the B-domain, the Z-domain, has been constructed for high-level protein expression (*15*) and, recently, has been minimized to two helices (33 residues) connected by a type I β-turn. This 2-helix fragment largely retains the binding affinity of the parent B-domain toward the Fc-portion of IgG (*16*−*17*).

In this study, we have replaced the type I β-turn of this minidomain with an elastin β-turn and have shown that the elastin sequence acts as a temperature switch. The minidomain with the elastin-turn binds the Fc of mouse IgG2a with an improved affinity at higher temperatures. At the same temperatures, the wild-type minidomain undergoes the expected decrease in affinity as it unfolds. This demonstrates that short elastin sequences when inserted into globular proteins have the ability to induce structure at higher temperatures, opening up the possibility of a general method for introducing controlled temperature regulation of protein function.

EXPERIMENTAL PROCEDURES

Peptide Synthesis. The synthesis was carried out by Synt:em (Nîmes, France) on an Automated Multiple Peptide Synthesis instrument (AMS 422, ABIMED) using a Fmoc solid support protocol (poly(ethylene glycol) grafted polystyrene support). The Fmoc amino acids were activated in situ by diisopropylcarbodiimide and 1-hydroxybenzotriazole in DMF with a standard 4-fold excess. An acetylation step was carried out after each amino acid incorporation to cap possible remaining amine groups and to ensure the absence of deletion peptides. The Fmoc protecting groups were removed by a solution of piperidine in DMF (20%) prior to each coupling, and after synthesis the peptide was cleaved from the support by a standard TFA cocktail, ether-precipitated, and purified on a Waters Prep LC 4000 System using Waters PrepPak Cartridge column C18, 6 μM, 60 Å (40 × 100 mm) and a gradient from A (0.1% TFA in water) to 60% B (0.08% v/ TFA in acetonitrile) in 60 min (flow 20 mL/min). Peptides were detected at 215 and 280 nm. The purity was confirmed using a Beckman LC126 HPLC system, with a Kromasil column C18, 5 μm, 100 Å (250 × 4.6 mm) applying a gradient from 95% A to 100% B in 15 min (flow 3.0 mL/min). The purity was further evaluated by mass spectroscopy analysis using a Maldi-tof spectrometer (Voyager DE Elite, PE Applied Biosystems) with dihydroxybenzoic acid as matrix.

Circular Dichroism Studies. The secondary structure of the minidomain constructs was analyzed by recording CD spectra on Jobin-Yvon Model CD6 Dichrograph Instrument (Instruments S. A. UK Ltd., Stanmore, UK). The instrument was iso-andosterone calibrated according to the manufacturers instructions, and it was temperature-controlled and N_2 purged during analysis. The minidomains were dissolved in sterile filtered (0.22 μm) solutions prior to analysis. Spectra were recorded from 190 to 260 nm with a step resolution of 0.5 nm (2.0 nm bandwidth), using an integration time of 1−5 s. The average of up to 4 runs were smoothed using the Sabitzky−Golay algorithm in the Dichrograph Software version 1.1 (Jobin-Yvon/Instruments S. A., France). Temperature CD scans were performed by a stepwise increase in temperature, from +1 °C and up, using a five minute equilibration time. The melting of the minidomains was monitored by integrating the molar ellipticity at 222 and 260 nm at each temperature for 10 s. The average of 3−6 measurements at each wavelength was used. The peptide stock concentrations (in deionized water) were determined by quantitative amino acid analysis. Data points at each wavelength were expressed as mean residual ellipticity ([θ], degree cm^2/dmol) by dividing the measured molar ellipticity by the number of residues in the minidomain.

Thermodynamic Analysis of CD-Data. The free energy for melting or folding of structure at 222 nm was fitted to a macroscopic, reversible, two-state model using the observed CD-data, $[\theta]^{222}$ and temperature, T. For folding (U→F) or melting (F→U) of structure, respectively, eqs 1 and 2 were used.

$$\Delta G_{U\rightarrow F} = -RT \ln[([\theta]^{222} - [\theta]^{U})/([\theta]^{F} - [\theta]^{222})] \quad (1)$$

$$\Delta G_{F\rightarrow U} = -RT \ln[([\theta]^{222} - [\theta]^{F})/([\theta]^{U} - [\theta]^{222})] \quad (2)$$

The pre- and post-transitional slopes for melting in TFE, respectively, mF and mU in eqs 3 and 4 below, used the data from WtSS and MutSS minidomains. For folding (U→F) in buffer, the respective slopes were similarly taken from WtOpen1 and WtOpen3 minidomains.

$$[\theta]^{F} = m\mathrm{F} \times T + \mathrm{off1} \quad (3)$$

$$[\theta]^{U} = m\mathrm{U} \times T + \mathrm{off2} \quad (4)$$

The offset values off1 and off2, together with ΔH and ΔS, were fitted for the melting curves of the minidomains. Where a mutant exhibited a less well-defined transition startpoint, datapoints were extrapolated based on the pre-transitional region of the wild-type minidomain in the same solvent. The heat capacity was set to zero since all minidomains were of relatively low molecular weight (~4000Da) [*11*, *18*, and references herein]. By replacing $[\theta]^{U}$ with $[\theta]^{F}$, and vice versa, in eqs 1 and 2, and 5 and 6, the thermodynamic values for the inverse transition, $\Delta G_{U\rightarrow F}$, were found.

$$\Delta G_{F\rightarrow U} = \Delta H_{F\rightarrow U} - T\Delta S_{F\rightarrow U} \quad (5)$$

$$[\theta]^{222} = ([\theta]^{F} + [\theta]^{U} \times \exp -(\Delta G_{F\rightarrow U}/RT))/(1 + \exp -(\Delta G_{F\rightarrow U}/RT)) \quad (6)$$

The data were fitted to either eq 1 or 2, together with eqs 3−6, using the least-squares method in the Grafit software (*19*).

Surface Plasmon Resonance Spectroscopy. Interaction kinetics of the minidomains (analytes) with immobilized Fc (ligand) was monitored by surface plasmon resonance spectroscopy using either BIAcoreX or BIAcore2000 (Biosensor, Sweden). The BIAcore 2000 was used for analyses of WtSS and MutSS minidomains over the temperature range +5° to +37 °C. Purified Fc prepared from the IgG2a mouse

monoclonal antibody 561 (antiCD34), a gift from Dynal A/S (Norway), and human serum albumin (HSA, Novo Nordisk, Denmark) were immobilized on a research grade CM-5 carboxymethylated sensor chip in 10 mM sodium acetate buffer pH 4.5 using the amine coupling kit with *N*-ethyl-*N*′-[(dimethylamino)propyl] carbodiimide (EDC) and *N*-Hydroxysuccinimide (NHS) provided by the manufacturer. The Fc of the mAb 561 (10 μL of 5 μg/mL) and HSA (10 μL of 10 μg/mL) were immobilized at +25 °C in the BIAcore2000 with a flow rate of 10 μL Hepes buffered saline (HBS; 10 mM Hepes pH 7.4, 150 mM NaCl, 3.4 mM EDTA) containing 0.005% (v/v) surfactant per minute. This gave 3100 and 3400 Ru's respectively after blocking with 1M ethanolamine pH 8.5 and regeneration using 5 μL 10 mM glycine·HCl buffer pH 2.4. Interaction analyses were performed with a flow rate of 30 μL/min in HBS/P20 (running buffer). Each minidomain (100 μL) was injected, using the KINJECT command, over a range of concentrations − between 4 and 10 different concentrations, depending on the experiment. The binding of the minidomains to Fc-561 was corrected by subtracting the RU's at the HSA portion of the chip (due to bulk-effects). The surface was regenerated prior to each injection with glycine·HCl pH 2.4. The data for the association constant was sampled by diluting each minidomain in running buffer to obtain several low concentrations, and the dissociation constant was determined from the highest concentration to minimize rebinding.

Evaluation of BIAcore Data. The k_{on} and k_{off} values were fitted by evaluating the sensorgram data using the BIAevaluation 2.1 software (Pharmacia Biosensor). By nonlinear fitting of two exponentials, the two-component association phase for the model: 2 Minidomains + Fc561 + Fc561* → Minidomain−Fc561 + Minidomain−Fc561* (Fc561 and Fc561* are two independent epitopes on Fc561), was found from eq 7,

$$R = R_A(1 - \exp(-ks_A t)) + R_B(1 - \exp(-ks_B t)) \quad (7)$$

where R is the response at time, t, and R_A and R_B are steady-state response levels for the two events. To determine the on-rates, the fitted values for ks_A and ks_B were plotted against minidomain concentration C. By using the relations $ks_A = k_{onA}C + k_{offA}$ and $ks_B = k_{onB}C + k_{offB}$, the k_{on}-rates for the parallel associations were found from the slope of a linear fit of ks_A or ks_B against C. The k_{on} - rate, which had its largest value, i.e., the fastest rate-constant (k_{onA} extracted from ks_A), was used for further calculation. The off-rates were determined for the two component interaction (parallel dissociation of two complexes) from the following:

$$R = R_D \exp(-k_{offA} t) + R_E \exp(-k_{offB} t) \quad (8)$$

R_D and R_E are the contributions of each component to the total response at the start of dissociation. However, only the fitted k_{offA} and k_{offB} were further used by specifying the start of dissociation at $t = t_0$. Again, the k_{off} - rate, which had its largest value, i.e., the fastest off-rate (k_{offA}), was used for further calculation. The dissociation constants were determined from the relation $K_D = k_{off}/k_{on}$. The relative differences in free energy of binding, $\Delta\Delta G$, between the different minidomains over the temperature ranges examined were calculated from:

$$\Delta\Delta G = +RT_x \ln[K_D(\text{mutant minidomain}) \text{ at } T/K_D (\text{wild-type minidomain}) \text{ at } T] \quad (9)$$

where R is the molar gas constant, T is the temperature (in Kelvin) and the K_D values are those based on the fast on- and off-rates.

RESULTS

The engineering of the small binding protein selected for this study, so that it was capable of being reversibly modulated by temperature changes, used an inter-helix turn replacement strategy in which the wild-type turn was replaced by the elastin sequence, GVGVPGVG (*11*). The minidomain derived from the B-domain of Protein A (*16*) was the model protein used (Figure 1, WtOpen). This minidomain is 33 residues long, is amenable to peptide synthesis, and binds the Fc region of IgG. We replaced the wild-type β-turn HDPNLN with the elastin sequence GVPGVG. We omitted the GV portion at the N-terminal start of the turn because it was flanked by the similar dipeptide AL (*AL*HDPNLN). However, we were concerned that the charge from the EE residues at the C-terminal end of the turn (HDPNLN*EE*) would elevate the transition temperature of the elastin sequence beyond 37 °C (*11*) and so we replaced EE with QQ in one construct (Figure 1, MutOpen1 and MutOpen3). Minidomains with a disulfide bond were also synthesized (Figure 1, WtSS and MutSS), since the wild-type S−S minidomain has been shown to be more thermostable and exhibit better Fc-binding than the open form (*17*). The minidomain purities and molecular masses (Syntem, France; see Experimental Section) were respectively: WtOpen (95%, 4122.0 Da), MutOpen1 (95%, 3879.3 Da), MutOpen2 (98%, 3879.7 Da), MutOpen3 (95%, 3881.5 Da), WtSS (97%, 4181.8 Da), and finally MutSS (96%, 3956.3 Da).

Structural Characterization of Minidomains by Circular Dichroism. The minidomains were scanned by far-UV circular dichroism in phosphate buffer at a low temperature in order to study the effect of mutations in the turn-region (Figure 2). Only the wild-type minidomains (WtOpen and WtSS, Figure 1) had characteristic α-helical CD-spectra with minima around 208 and 222 nm and a maximum around 190 nm. The relatively low-CD-amplitude (MRE around −10 000 deg cm^2 dmol^{-1}) for WtOpen indicated that this existed only as a partially folded α-helical structure (20, and references herein). However, the WtSS minidomain had a higher helical content—probably due to the additional stabilization introduced by the S−S bridge. More surprising was the observation that all mutants with the elastin β-turn were largely unstructured at the low temperature, although MutOpen2 with a protected C-terminus, had a higher helix content in phosphate buffer (measured at 222 nm) than the other mutants.

The effect of TFE, known to have a stabilizing effect on α-helices (*21*−*22*), was tested on all minidomains. It was observed that TFE stabilized or induced α-helix structure in all minidomains, illustrated for WtSS and MutSS in Figure 3. By increasing the concentration of TFE in phosphate buffer, a CD-transition from random coil to an α-helical spectrum was seen for MutSS, with a near isodichroic point around 204 nm (Figure 3B). Similar spectra were obtained

WtOpen	NH_2-F[6]NMQQQRRFYEAL**H[19]DPNLNEE[26]**QRNAKIKSIRDD[38]-COO^-
MutOpen1	NH_2-F[6]NMQQQRRFYEAL**G[19]VPGVGQQ[26]**QRNAKIKSIRDD[38]-COO^-
MutOpen2	NH_2-F[6]NMQQQRRFYEAL**G[19]VPGVGEE[26]**QRNAKIKSIRDD[38]-$CONH_2$
MutOpen3	NH_2-F[6]NMQQQRRFYEAL**G[19]VPGVGEE[26]**QRNAKIKSIRDD[38]-COO^-
WtSS	NH_2-F[6]NMQ**C**QRRFYEAL**H[19]DPNLNEE[26]**QRNAKIKSIRDD**C**[39]-COO^-
MutSS	NH_2-F[6]NMQ**C**QRRFYEAL**G[19]VPGVGQQ[26]**QRNAKIKSIRDD**C**[39]-COO^-

FIGURE 1: Sequences of short IgG-binding minidomains derived from Protein A. The minimized IgG-binding B-domain of protein A (*16*) was synthesized (WtOpen), and the turn-region mutants (residues 19−26) based on the elastin sequence GVPGVG are also shown (MutOpen 1−3). Minidomains with disulfur bond (*17*) were also synthesized. Both the wild-type minidomain, WtSS, and its mutant minidomain, MutSS, have an S−S bond between Cys10 and Cys39.

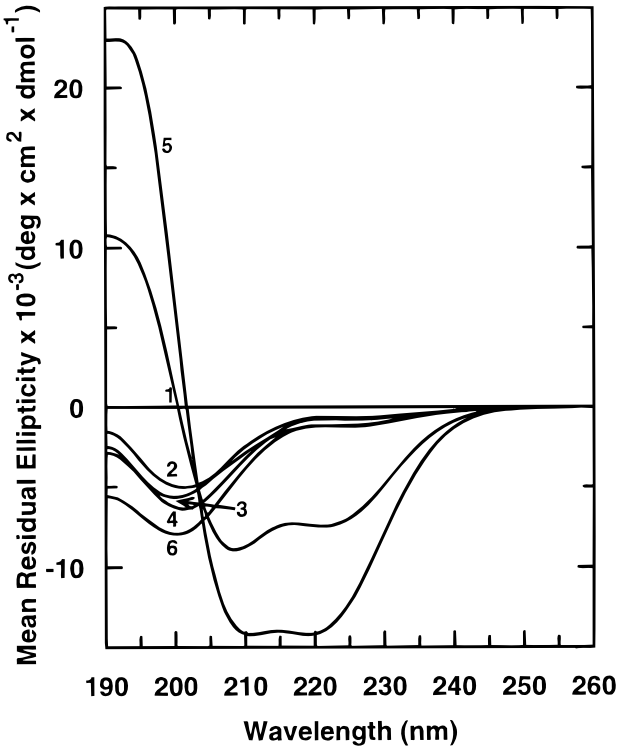

FIGURE 2: Circular Dichroic wavelength scans of minidomains in phosphate buffer pH 7.0 or in deionized water. The minidomains were scanned once in 10 mM buffer at +6.4 °C using a 0.2 cm stoppered cuvette with 5 s integration time (0.5 nm steps; slit: 2.0 nm). WtSS and MutSS were scanned in deionized water. The different spectra with their respective minidomain concentrations are respectively: WtOpen (1; 21.4 μM), MutOpen1 (2; 26.9 μM), MutOpen2 (3; 29.7 μM), MutOpen3 (4; 21.1 μM), WtSS (5; 24.3 μM) and MutSS (6; 25.1 μM).

for MutOpen1−3 (not shown). This demonstrated that all mutants possessed an α-helix propensity, even though they were largely unordered in phosphate buffer. The CD-spectra of the wild-type minidomains in phosphate buffer reflected a greater α-helical content with increasing concentrations of TFE (Figure 3A and 3C). At about 20% (v/v) TFE, the transition seemed to be complete, while for the mutant minidomains the maximum effect of TFE was seen at 30%. However, when the concentration of TFE was increased above 20% for wild-type minidomains (WtOpen and WtSS), the CD-signal at 222 nm was diminished. The sigmoid profiles of the CD-curves, with an inflection point at about 20% TFE, suggests that cooperative interactions are involved

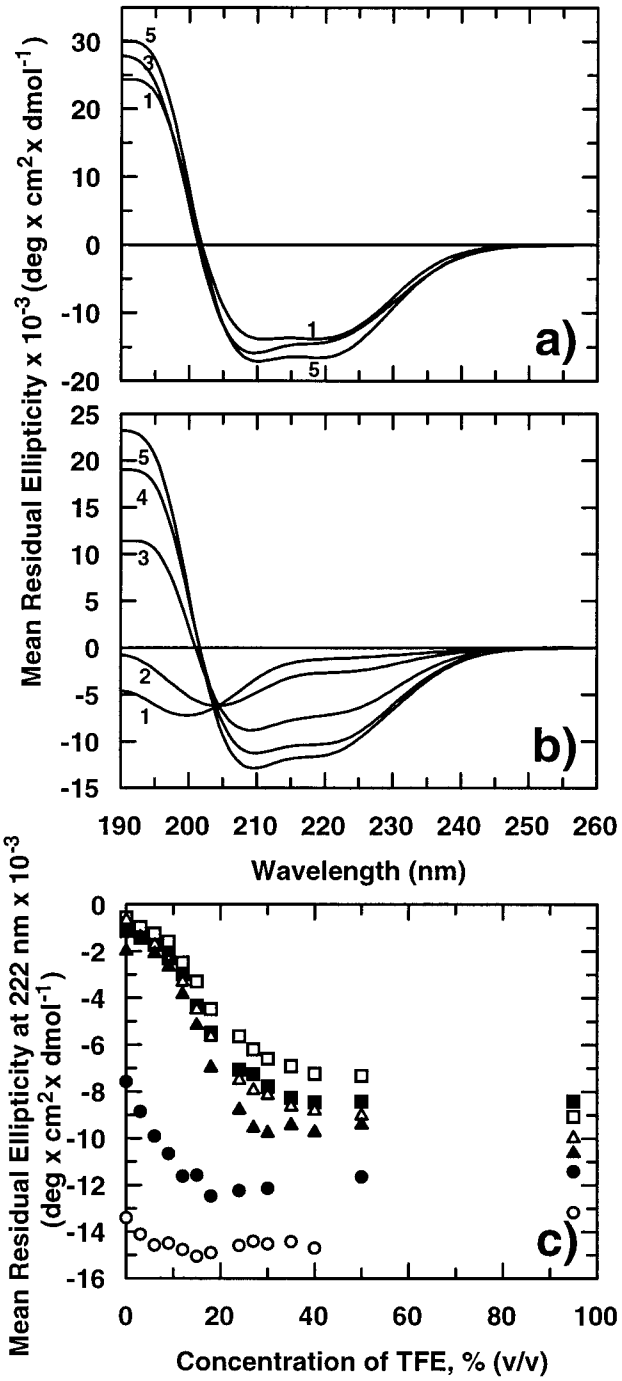

FIGURE 3: The concentration effect of Trifluoroethanol (TFE) on the minidomains. The effect of increasing concentrations of TFE in phosphate buffer on WtSS (a) and MutSS 6 (b) is shown. The numbers represent increasing concentrations of TFE: 1, 0% TFE; 2, 9% TFE; 3, 18% TFE; 4, 27% TFE; 5, 95% TFE. The minidomains were scanned once at +6.4 °C and the experimental conditions and minidomain concentrations were the same as described in Figure 2. The effect on the mean residual ellipticity at 222 nm for WtOpen (●), MutOpen1 (□), MutOpen2 (■), MutOpen3 (△), WtSS (○), and MutSS (▲) is illustrated in panel c.

in this transition. At 50% TFE, the helix content of the minidomains was in the order: WtSS > WtOpen > MutSS > MutOpen2 = MutOpen3 > MutOpen1.

For all minidomains the temperature-dependent CD scans in TFE were 95−100% reversible after cooling (not shown, but see ref *17*). The observed near isodichroic point at 204 nm also indicated that the melting of the α-helices in TFE

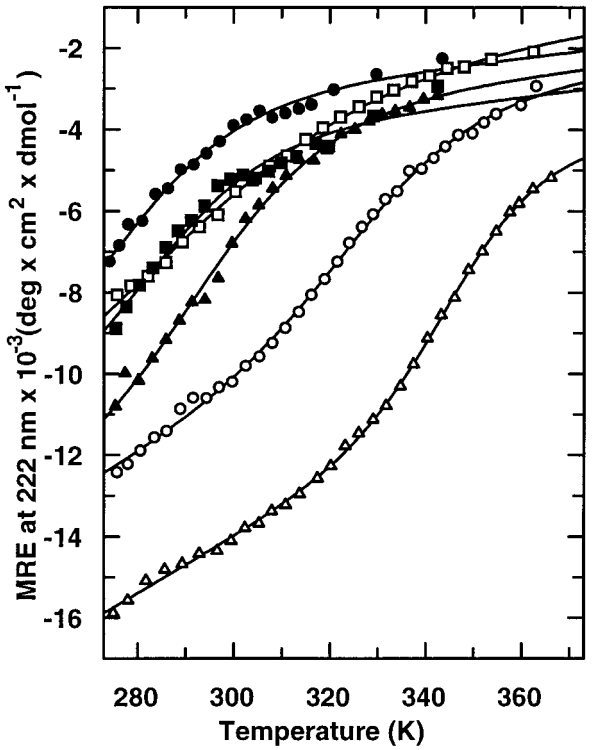

FIGURE 4: The temperature effect on minidomains in 30% trifluoroethanol (TFE). The melting of the minidomains was followed at 222 nm using the average of three independent scans with an integration time of 5 s (in 0.2 cm cuvette, slit: 2.0), and the temperature effect on minidomains in 30% (v/v) TFE are shown. Respectively, WtOpen (○), MutOpen1 (●), MutOpen2 (□), MutOpen3 (■), WtSS (△), and MutSS (▲). The data were fitted to a two-state transition with slopes (see methods). WtSS and MutSS were fitted with fixed pre and posttransitional slopes.

Table 1: Thermodynamic Values for Melting of Minidomains in 30% (v/v) Trifluoroethanol[a]

minidomain	T_M (°C)	ΔH (kcal mol^{-1})	ΔS (kcal mol^{-1} K^{-1})
WtOpen	58	15.4 ± 1.0	0.046 ± 0.003
MutOpen1	10	12.0 ± 0.7	0.042 ± 0.003
MutOpen2	33	7.4 ± 0.4	0.024 ± 0.001
MutOpen3	16	12.9 ± 1.4	0.045 ± 0.005
WtSS	75	23.9 ± 1.0	0.069 ± 0.003
MutSS	26	12.8 ± 0.6	0.043 ± 0.002

[a] The mean residual ellipticity was followed at 222 nm for each minidomain and then fitted to a reversible van't Hoff equation with $\Delta Cp = O$ allowing ΔH and ΔS to float. The pre- and posttransitional slopes were fixed at the same values for all minidomains, and the pretransitional region for the mutants (MutOpen1-3 and MutSS) was extrapolated, based on the observed data for their respective wild-type minidomains, WtOpen and WtSS.

for the minidomains followed a two-state reversible α-helix-coil transition (Figure 3B). To quantify the effect of the mutations in the turn region, α-helix structure was first induced in all minidomains using TFE (30%) and their melting was then followed at 222 nm (Figure 4).

Further analysis of the melting curves was performed by fitting the data to a reversible van't Hoff two-state transition. Table 1 displays the thermodynamic data for the different minidomains in 30% TFE. Compared to WtOpen the T_M was lowered by 25 °C and 42 °C for MutOpen2 and MutOpen3, respectively and by 48 °C for MutOpen1. The wild-type disulfide-stabilized minidomain WtSS was 49 °C more stable than its mutant partner, MutSS. The difference in stability between WtOpen and MutOpen1 and between WtSS and MutSS shows that the GVPGVG-turn lowers the stability of the helices irrespective of the presence of a disulfide bond, notwithstanding the fact that the disulfide bonded minidomains were already 16−17 °C more stable than the open forms. The stability difference between the open form and S−S stabilized wild-type minidomains in Tris buffer has previously been reported as 40 °C (*17*), and for S−S stabilized laminin helices it was around 18 °C (*23*). These results confirmed that MutOpen1 was the least, while WtSS was the most thermostable.

There were no large differences in ΔH or ΔS values observed for the open form mutants and the corresponding S−S constructs, indicating that the thermodynamic effect of TFE was the same for both forms (both minidomains were initially melted in 0% TFE). Interestingly, WtSS had larger values for ΔS and ΔH in TFE relative to WtOpen reflecting the influence of a stabilizing S−S bond on the energetics of a helix-stabilizing trifluorethanol system.

For WtOpen and WtSS minidomains, the CD-amplitude decreased with increasing temperature in HBS as shown for WtSS in Figure 5A. The same behavior was seen in TFE, phosphate buffer, micellar SDS, and sodium sulfate at higher temperatures (not shown). However, in contrast to the wild-type behavior, the melting curves for the mutants in HBS, phosphate buffer or water had an increased CD-amplitude at 210−260 nm with increasing temperature and a near isodichroic point at 210 nm, as shown for MutSS in Figure 5B. All transitions were 90−100% reversible as is illustrated in Figure 5. A, B, and C. The MRE at 222 nm was followed for MutOpen1−3, MutSS and WtSS in 10 mM phosphate buffer, and HBS with increasing temperature, and the melting curves for WtSS and MutSS in HBS are shown in Figure 5C. Their sigmoid profiles are consistent with the occurrence of a cooperative transition. The data were fitted to a two-state reversible transition in the direction folded to unfolded for WtSS, or to the reverse transition for MutOpen1, MutOpen3, and MutSS.

The concentration dependence of the spectra at 15.5 and 48 °C in phosphate buffer was also tested for selected minidomains (up to 620 μM; data not shown). For MutSS the concentration was taken from 15 μM to 1.8 mM in the BIAcore running buffer (HBS with 0.005% (v/v) P20) at 25 °C without any significant deviations at 222 nm (not shown). By equilibrium ultracentrifugation of WtSS and WtOpen, it has previously been shown that they are monomeric and highly soluble (*17*). In addition, short to intermediate (8−23) GVPGVG-based peptides have also been shown to be concentration independent at elevated temperatures (*11*).

The melting of MutOpen2 exhibited unusual behavior in which increased and decreased MREs at 222 nm were seen (not shown). For this reason, only the thermodynamic data for MutOpen1, MutOpen3, and MutSS are given in Table 2. The van't Hoff plots were linear with correlation coefficients on the average of −0.98 (not shown). The energies involved in the transition (Table 2) were lower than for the melting of WtSS in HBS ($\Delta H = 20.8$ kcal mol^{-1} and $\Delta S =$ 0.063 kcal mol^{-1} K^{-1}) and of similar magnitude to those observed for folding of individual GVGVPGVG-peptides (*11*).

Evaluation of Minidomains by Surface Plasmon Resonance. The kinetics of minidomain binding to immobilized

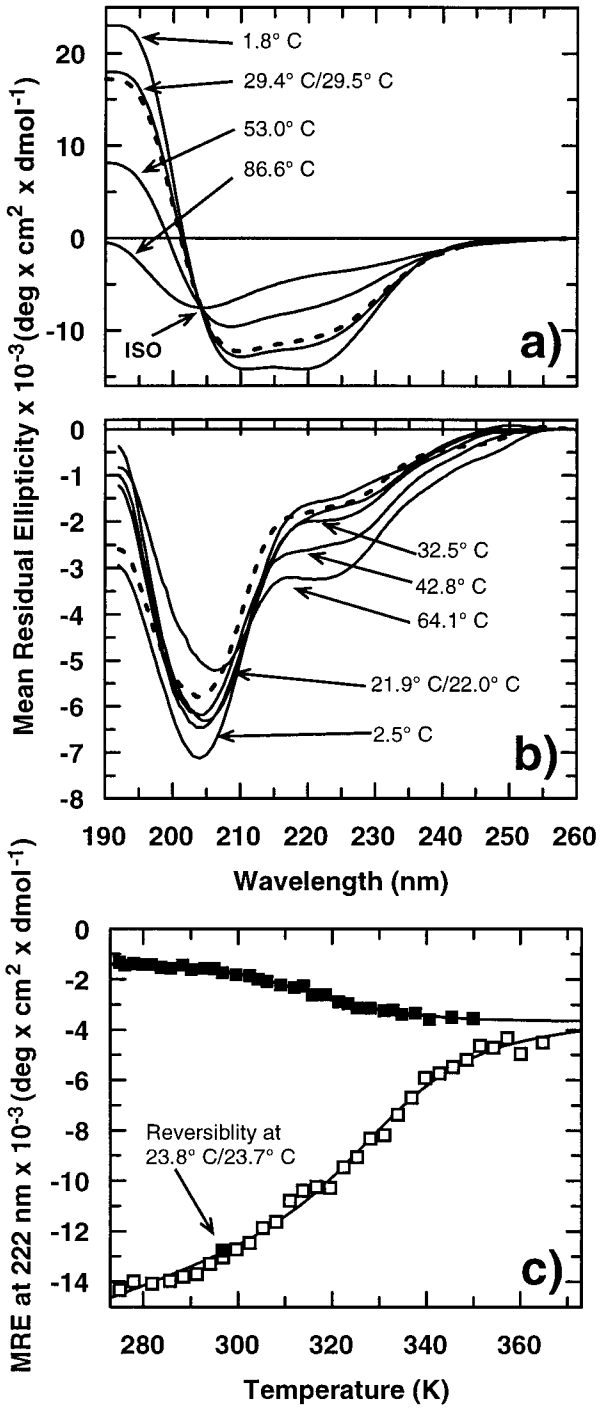

FIGURE 5: Temperature CD-wavelength scans of WtSS and MutSS minidomains in deionized water and in HBS with 0.005% (v/v) P20. WtSS (24.3 μM) in deionized water was scanned once from 190 to 260 nm (0.2 cm quartz cuvette with 5 s integration time; slit 2.0 nm; 0.5 nm step size) at different temperatures, as displayed in panel a. Similarly MutSS (350.7 μM) in Hepes-buffered saline added 0.005% surfactant P20 (panel b) was scanned from 192 to 260 nm at different temperatures using a 0.1 mm stoppered cuvette. The bold dashed lines (---) illustrate the reversibility of the scans after being heated to 60−80 °C and then by rescanning the minidomains at the temperature *x*, (../*x*) given in the plots. Panel c shows the melting of WtSS (□; 24.3 μM) and MutSS (■; 25.1 μM) in HBS buffer with P20. The melting was followed by measuring the CD-ellipticity at 222/260 nm (in 0.2 cm cuvette, slit: 2.0 nm) at different temperatures averaging three independent scans with an integration time of 5 s.

Fc was studied using the BIAcoreX and BIAcore 2000 (BIAcore, Sweden). The data generated were fitted both to a one-component model:

$$\text{Minidomain} + \text{Fc561} \rightleftarrows \text{Minidomain}-\text{Fc561}$$

and to a two-component model:

$$2\ \text{Minidomains} + \text{Fc561} + \text{Fc561*} \rightleftarrows \text{Minidomain}-\text{Fc561} + \text{Minidomain}-\text{Fc561*}$$

where Fc561 and Fc561* represent two different epitopes on the ligand. The goodness of these fits is illustrated for WtSS at 20 °C in Figure 6, A and B. There was generally a better fit (lower χ^2) to a two-component model over the temperature ranges tested, for both the association and dissociation phases. The on-rates were measured from the slope of a linear fit of the ks_A or ks_B values vs the lowest concentrations used, illustrated for WtSS and MutSS, respectively, in Figure 6C and 6D (inserts). The ks_A-values represent the fastest rate-constant relative to ks_B. The linear correlation coefficient (r) for the secondary fit of the fast on-rates was around 0.98. By contrast, the slower on-rates (k_{onB}) were approximately 50-fold lower in magnitude and generally exhibited much larger variability at the elevated temperatures. At the lower temperatures, however, both the fast and slow off-rates were statistically determined for WtOpen and MutOpen, and also at all temperatures for WtSS and MutSS (not shown). The dissociation constants ~200 nM for WtOpen and ~100 nM WtSS using the slow off-rates (0.04 s^{-1} and 0.02 s^{-1} respectively at +10 °C/+5 °C) were very similar to those previously reported (*17*). However, it has to be stressed that the systems are different. In this report, the association of the minidomain to the Fc of a mouse IgG2a (561) was studied, while Starovasnik et al. (*17*) and Braisted and Wells (*16*) studied binding to a human IgG1.

The temperature-dependent progress curves for binding and dissociation of WtSS (Figure 6C) and MutSS (Figure 6D) to immobilized Fc of the mouse monoclonal IgG2a are shown in Figure 6C and Figure 6D, respectively. Interestingly, there was a reverse temperature effect for the binding of MutSS relative to WtSS (Figure 6, C and D and Figure 7, A, B, and C). The fast off-rates for WtOpen, MutOpen1 and WtSS increased with increasing temperature (only shown for WtSS), while over the same temperature range the mutant MutSS had a lowered off-rate (Figure 7A). The slow off-rates did not vary much for the minidomains over the temperature range tested, but both the fast and slow off-rates decreased for MutSS from 5 to 37 °C (not shown). The slow off-rates for the MutSS were also lower than for

Table 2: Thermodynamic Data for Inverse Thermal Transition at 222 nm for Mutant Minidomains in Buffers[a]

	T_M (°C)	ΔH (kcal mol^{-1})	ΔS (kcal mol^{-1} K^{-1})
MutOpen1 in phosphate buffer	21	16.5 ± 1.1	0.056 ± 0.004
MutOpen1 in HBS with P20	32	14.4 ± 1.8	0.047 ± 0.006
MutOpen3 in phosphate buffer	46	16.4 ± 1.2	0.051 ± 0.004
MutOpen3 in HBS with P20	43	12.1 ± 1.5	0.038 ± 0.005
MutSS in HBS with P20	42	18.4 ± 1.1	0.059 ± 0.003
GVG(VPGVG) peptides[b]		16.8	0.056

[a] The melting data at 222 nm was fitted to a reversible van't Hoff equation allowing ΔS and ΔH to float. All data were fitted with fixed pre- and posttransitional slopes. The heat capacity was fixed at 0. [b] (*11*); the values are the average of short $GVG(VPGVG)_n$ peptides ($n = 1$ and 3) in 10 mM phosphate buffer pH 7.0.

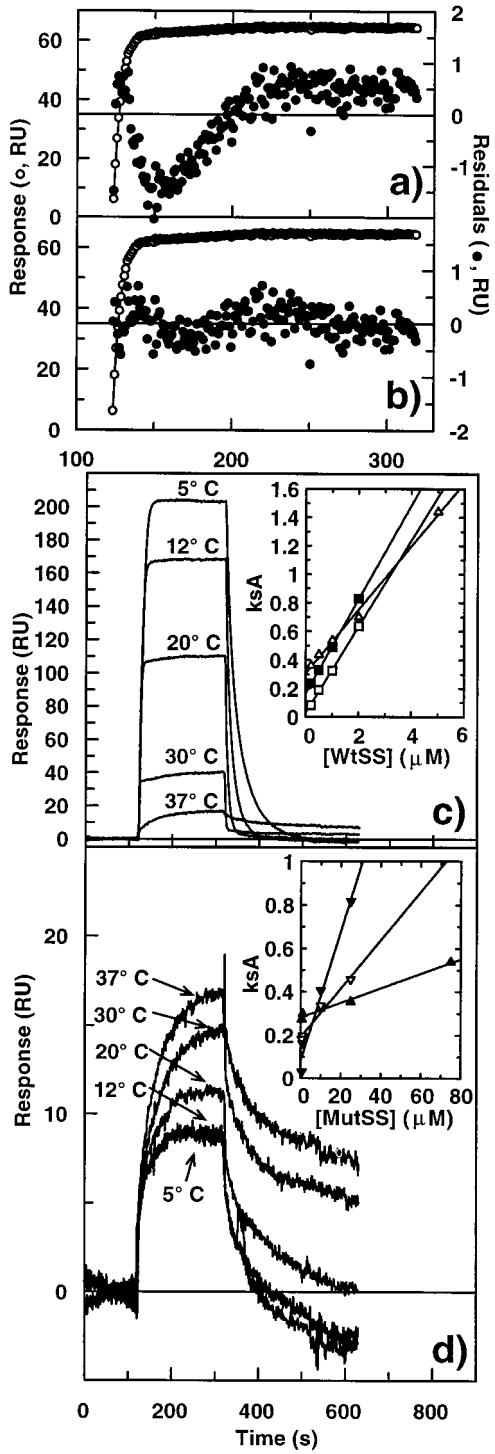

FIGURE 6: BIAcore fits and progress curves for WtSS and MutSS. The association between 200 nM WtSS and immobilized Fc of 561 (mouse monoclonal IgG2a) at 20 °C was fitted to a WtSS + Fc561 ⇄ WtSS−Fc561 model using BIAevaluation 2.1 software (panel a). The χ^2 for the fit was 0.556. Panel b represents the fit to the model: 2 WtSS + Fc561 + Fc561* ⇄ WtSS−Fc561 + WtSS−Fc561* where one WtSS minidomain reacts with 2 independent sites on Fc561. The χ^2 for this fit was 0.0795. The lines show the fit of raw-data (○), and residuals for the model (●). The BIAcore progress curves for binding of minidomains to Fc561 at different temperatures are shown for 500 nM WtSS in (panel c) and for 1 μM MutSS in d. The plots of their respective fast on-rates, ks_A (see methods) vs minidomain concentrations are illustrated in the inserted panels in c for WtSS (□, 12 °C; ■, 20 °C and △, 37 °C) and in d for MutSS (▲, 12 °C; △, 25 °C and ▼, 37 °C).

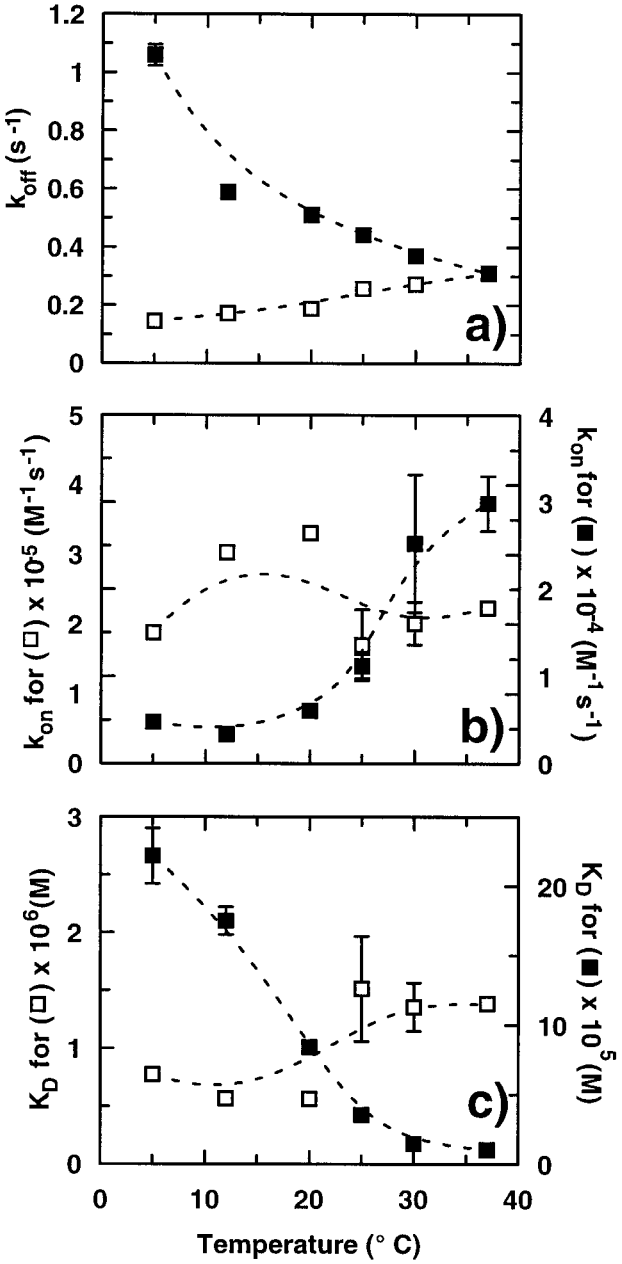

FIGURE 7: The temperature dependence of the fast kinetic constants for WtSS and MutSS minidomains. The respective kinetic constants for the S−S linked minidomains WtSS (□) and MutSS (■) are in panel a, b and c. Panel a shows the fast off-rates, panel b the fast on-rates and panel c illustrates their respective fast dissociation constants ($=k_{off}/k_{on}$) at different temperatures. The k_{on}-rates were found from the slopes of the plots of ks_A vs minidomain concentration, as is illustrated in Figure 6, C and D (inserts) for the model Minidomain + Fc561 + Fc561* ⇄ Minidomain−Fc561 + Minidomain−Fc561*. The off-rates were determined from the model Minidomain$_i$Fc561$_i$ ⇄ Minidomain$_i$ + Fc-561$_j$ (parallel dissociation of two complexes). The off-rates were fitted using BIAevaluation 2.1 and the on-rates were fitted using both BIAevaluation 2.1 and GRAFIT (*19*). Both the on-rates and off-rates display their fitted standard errors. The standard errors of the dissociation constant were manually calculated based on SEs for k_{on} and k_{off}.

WtSS (respectively ~0.01 s^{-1} versus ~0.02 s^{-1}), which is surprising considering the lower residual structure in this minidomain. Again, there was only a small variation in the on-rates for WtSS over the temperature range applied. For MutSS however, the on-rate tripled on increasing the temperature from 5 to 37 °C (Figure 7B). Similar effects

were seen with WtOpen and MutOpen1 whose on-rates halved and doubled, respectively, over the temperature range 10−30 °C (data not shown). The overall effect of these changes is exemplified by the behavior of the MutSS minidomain, whose increased fast on-rate and lowered fast off-rate at 37 °C improved its affinity some 21-fold, compared with that observed at 5 °C (K_D reduced from 222 to 10.4 μM) (Figure 7C). Using the slow off-rates, MutSS also improved its affinity by 8-fold (from 2.8 to 0.4 μM) in the same temperature range.

In contrast, for the WtOpen minidomain (without S−S bridge) the K_D increased 8-fold over the same temperature range, while for WtSS (with S−S bridge) the K_D was unchanged (using either the slow or fast off-rates).

Free-Energy Differences. The $\Delta\Delta G$ values vs temperature had a better linear fit for WtOpen and MutOpen1 (correlation coefficient $r = -0.99$) than for WtSS and MutSS ($r = -0.96$). Over the temperature range measured, $\Delta\Delta G$ was positive for both minidomain pairs, indicating that the binding of wild-type to Fc was tighter than that of the mutants. However, over the same temperature range $\Delta\Delta G$ decreased by 0.057 kcal mol^{-1} K^{-1} for MutOpen1 relative to WtOpen, and by 0.090 kcal mol^{-1} K^{-1} for MutSS relative to WtSS. The $\Delta(\Delta\Delta G)$ was lowered, respectively, by 1.2 kcal mol^{-1} (20 K) for MutOpen1 or by 2.9 kcal mol^{-1} (32 K) for MutSS relative to the wild-type partners. If this relationship were to hold over a wider temperature range, then it predicts that the affinity of MutOpen1 would exceed that of WtOpen beyond 81 °C, while that of MutSS would exceed the affinity of WtSS beyond 49 °C.

DISCUSSION

We report here the first example of the introduction of an elastin-like sequence into the primary structure of a globular protein. Previously, we have shown that short elastin peptides can undergo an entropically driven transition from an extended to a type II β-turn, mimicking the behavior of the much longer, naturally occurring elastin molecule (*11*). By increasing the hydrophobicity in the turn-region, the probability of formation of the turn containing the elastin GVPGVG sequence should increase with increasing temperature. In this design, the wild-type β-turn (type I) residues were replaced with the helix-destabilizing Val, Gly, and Pro residues, while the native Glu−Glu sequence adjacent to the turn was mutated to Gln−Gln in order to avoid an abnormally high transition temperature (*11*). Making such a change, thus, ran the risk of affecting the helix stability, since Val, Gly, and Pro are known to have a low helix propensity although Gln is more stabilizing than Glu (*24*).

The substitution of the type I β-turn by the more hydrophobic elastin turn resulted in melting of the helical structure of the wild-type minidomain in phosphate buffer. However, even the wild-type minidomain is unstable per se and stabilization by a disulfide-bridge at the termini was found to be necessary (*17*). Stabilizing α-helices in TFE also offers a way of expressing the difference in intramolecular stability between mutant and wild-type α-helical minidomains where the helicity of the mutants is more or less lost. This is illustrated for MutOpen1 and MutSS whose melting temperatures were decreased by about 48 °C in 30% TFE compared to wild-type WtOpen and WtSS minidomains (Table 1). MutOpen2 and MutOpen3, which retained the Glu25−Glu26 sequence close to the turn, were more helical in TFE than the Gln25−Gln26 sequences and their T_M's were lowered by only 25−42 °C. This unexpected effect may be due to stabilizing interactions with positively charged residues (Arg28 or Lys31) located close to the turn.

A helix stabilizing effect was seen for MutOpen2 that contained an amidated C-terminus (Table 1), an effect that has previously been shown for α-helices (*25*). The CD-amplitudes for MutOpen1−3 and MutSS, in phosphate buffer or in HBS containing P20, increased at 222 nm with increasing temperature, signaling the formation of an α-helix or type I β-turn (*26*−*27*). The shift of the isodichroic point from 204 to 210 nm, and the lower intensities of the CD-signals at 222-nm for the melting curves in buffer, were more characteristic of a type I β-turn (*27*). Several other observations also argue that a type I β-turn was formed at the higher temperatures. Type I β-turn structures have also been found in elastin sequences (*12*−*13*) although the Pro−Gly type II β-turn is between 0.2 and 1.7 kcal mol^{-1} more stable than type I β-turn and is also more common in elastin (*6*, *28* and references therein). A conformational interconversion between type I and II β-turn in proteins is, however, quite common for Pro−Gly turns (*29*).

The energies associated with the observed transitions for MutOpen1, MutOpen3, and MutSS (Table 2) were similar to those found for short (8−12 residue) elastin peptides (*11*). The melting of MutOpen1 over the temperature range 0−60 °C involved a free energy difference of 3.0 kcal mol^{-1}, within the range reported to be required for β-turn formation (2−4 kcal mol^{-1}) though just below that required for α-helix formation (4 kcal mol^{-1}; *28* and references herein).

The better fit of the BIAcore data to a heterogeneous kinetic model may be due to several factors. The minidomains were initially selected by panning against a human monoclonal IgG1 (*16*). In this system, we have studied the binding to the Fc-region of a mouse monoclonal IgG2a. It is possible that the panning of a specific binder to human IgG1 has selected for a species whose binding to related IgG epitopes is less promiscuous than the parent domain. This selection seems to have resulted in a weaker, heterogeneous binding behavior to IgG2a (the better fit to two Fc561 sites, Fc561, and Fc561*, is shown in Figure 6B). This may have implications for further design of antibodies by phage display—the choice between specificity or promiscuity. An alternative explanation is that the increased temperature may have generated different conformations of the epitopes on IgG2a due to structural instability, seen as a better fit of data to one-component kinetics at low temperatures and two-component kinetics at higher temperatures for some minidomains. Starovasnik et al. (*17*) also suggest two χ^1 rotamer conformations for Phe14 in the binding-site of the wild-type minidomain. Third, there may have been a mixed population of mutant domains, originating from the presence of multiple β-turns, although we think this unlikely.

The mutant minidomains MutOpen1 and MutSS in HBS showed a good correlation between on-rate and 2° structure content (measured by CD-amplitude at 222 nm) as temperature was increased. For MutSS a 21-fold improvement in K_D was obtained, due predominantly to the decrease in off-rate at the higher temperatures, an effect not seen for its open partner, MutOpen1. This was in stark contrast to the behavior

of wild-type WtSS which, although more thermostable, showed little variation in K_D over the same temperature range. This improvement in binding of the mutants with increasing temperature is, we believe, due to the formation of an entropy driven type I β-turn.

Other studies have shown a correlation between lowered α-helicity and lowered affinity (on-rates) of human insulin-like growth factor I (*30*). For Protein A Fc-binding domains, the residues involved in binding are known to be aligned on adjacent faces of two of the three helices (*17*). Any perturbation of these two helices will be likely to affect the affinity of the domain. This is clearly observed for the wild-type domains where denaturation of the helices mirrors loss of binding. However, in the mutant domains, the temperature induced formation of a type I β-turn (*17*) may serve to stabilize the alignment of fluctuating helices (reducing its conformational entropy relative to the wild-type), resulting in correctly positioned binding residues and a concomitant increase in affinity. As a matter of comparison, the formation of different turn conformations has also been shown to affect binding of the RGD-epitope to Integrins (*31*) and of inhibitor binding to HIV-1 protease (*32*).

There have been several previous attempts to alter the stability of proteins in a predictable manner by mutating residues in turn regions. Longer loops have been inserted without any significant effect on protein stability and folding, and residue substitutions have also been made (*33*−*35*). However, mutations of structurally important turns may still affect the function of a protein (*31*). The ability to control binding of Protein A by a temperature switch is a challenging task since its triple-helical core is normally quite thermostable. A switch that turns off the activity at low temperatures and turns it on again at higher temperatures may have several industrial applications, and in the particular example described here, may offer a novel temperature regulation for protein A. It may also become a general method for regulating other globular proteins where lowering the on-rate at lower temperatures and increasing it at higher temperatures leads to regulation of binding or some other activity.

ACKNOWLEDGMENT

We thank Dr. A. R. Clarke and the Department of Biochemistry, School of Medical Sciences, University of Bristol, for giving us access to a CD-machine. We also gratefully acknowledge Mrs. A. K. Lindgaard and Mrs. H. T. Trømborg at Dynal Core Tech. R & D for start-up help with BIAcoreX and BIAcore2000 measurements. Finally, we thank Dr. G. Bloomberg at School of Medical sciences, University of Bristol for amino acid analysis.

REFERENCES

1. Daughdrill, G. W., Chadsey, M. S., Karlinsey, J. E., Hughes, K. T., and Dahlquist, F. W. (1997) *Nat. Struct. Biol. 4*, 285−291.
2. Uesugi, M., Nyanguile, O., Lu, H., Levine, A. J., and Verdine, G. L. (1997) *Science 277*, 1310−1313.
3. van Stokkum, I. H. M., Lindsell, H., Hadden, J. M., Haris, P. I., Chapman, D., and Bloemendal, M. (1995) *Biochemistry 34*, 10508−10518.
4. Urry, D. W. (1988) *J. Protein Chem. 7*, 1−34.
5. Urry, D. W. (1988) *J. Protein Chem. 7*, 81−114.
6. Urry, D. W. (1993) *Angew. Chem. Int. Ed. Engl. 32*, 819−841.
7. Dill, K. A. (1990) *Biochemistry 29*, 7133−7155.
8. Head-Gordon, T. (1995) *Proc. Natl. Acad. Sci. U.S.A. 92*, 8308−8312.
9. Livingstone, J. R., Spolar, R. S., and Record, M. T., Jr. (1991) *Biochemistry 30*, 4237−4244.
10. Muller, N. (1993) *Biopolymers 33*, 1185−1193.
11. Reiersen, H., Clarke, A. R., and Rees, A. R. (1998) *J. Mol. Biol. 283*, 255−264.
12. Arad, O., and Goodman, M. (1990) *Biopolymers 29*, 1651−1668.
13. Bhandary, K. K., Senadhi, S. E., Prasad, K. U., Urry, D. W., and Vijay-Kumar, S. (1990) *Int. J. Pept. Protein Res. 36*, 122−127.
14. Uhlén, M., Guss, B., Nilsson, B., Gatenbeck, S., Philipson, L., and Lindberg, M. (1984) *J. Biol. Chem. 259*, 1695−1702 (Correction, ibid. p 13628).
15. Nilsson, B., and Abrahmsén, L. (1990) *Methods Enzymol. 185*, 144−161.
16. Braisted, A. C., and Wells, J. A. (1996) *Proc. Natl. Acad. Sci. U.S.A. 93*, 5688−5692.
17. Starovasnik, M. A., Braisted, A. C., and Wells, J. A. (1997) *Proc. Natl. Acad. Sci. U.S.A. 94*, 10080−10085.
18. Scholtz, J. M., Marqusee, S., Baldwin, R. L., York, E. J., Stewart, J. M., Santoro, M., and Bolen, D. W.(1991) *Proc. Natl. Acad. Sci. U.S.A. 88*, 2854−2858.
19. Leatherbarrow, R. J. (1989), Erithacus Software Ltd.
20. Luo, P., and Baldwin, R. L. (1997) *Biochemistry 36*, 8413−8421.
21. Cammers-Goodwin, A., Allen, T. J., Oslick, S. L., McClure, K. F., Lee, J. H., and Kemp, D. S. (1996) *J. Am. Chem. Soc. 118*, 3082−3090.
22. Jasanoff, A., and Fersth, A. R. (1994) *Biochemistry 33*, 2129−2135.
23. Antonsson, P., Kammerer, R. A., Schulthess, T., Hänisch, G., and Engel, J. (1995*) J. Mol. Biol. 250*, 74−79.
24. Chakrabartty, A., Kortemme, T., and Baldwin, R. L. (1994) *Protein Sci. 3*, 843−852.
25. Fairman, R., Shoemaker, K. R., York, E. J., Steward, J. M., and Baldwin, R. L. (1989) *Proteins: Struct., Funct., Genet. 5*, 1−7.
26. Perczel, A., Hollósi, M., Sándor, P., and Fasman, G. D. (1993) *Int. J. Pept. Protein Res. 41*, 223−236.
27. Woody, R. W. (1995) *Methods Enzymol. 246*, 34−71.
28. Yang, A.-S., Hitz, B., and Honig, B. (1996) *J. Mol. Biol. 259*, 873−882.
29. Gunasekaran, K., Gomathi, L., Ramakrishnan, C., Chandrasekhar, J., and Balaram, P. (1998) *J. Mol. Biol. 284*, 1505−1516.
30. Jansson, M., Uhlén, M., and Nilsson, B. (1997) *Biochemistry 36*, 4108−4117.
31. Bach, A. C., II, Espina, J. R., Jackson, S. A., Stouten, P. F. W., Duke, J. L., Mousa, S. A., and DeGrado, W. F. (1996) *J. Am. Chem. Soc. 118*, 293−294.
32. Nicholson, L. K., Toshimasa, Y., Torchia, D. A., Bax, S. H., Stahl, S. J., Kaufman, D., Wingfield, P. T., Lam, P. Y. S., Jadhav, P. K., Hodge, N., Domaille, P. J., and Chang, C.-H. (1995) *Nature Struct. Biol. 2*, 274−280.
33. Ladurner, A. G., and Fersth, A. R. (1997) *J. Mol. Biol. 273*, 330−337.
34. Predki, P. F., Agrawal, V., Brünger, A. T., and Regan, L. (1996) *Nature Struct. Biol. 3*, 54−58.
35. Viguera, A.-R., and Serrano, L. (1997) *Nature Struct. Biol. 4*, 939−946.

BI991243A